HHS Public Access

Author manuscript

J Craniomaxillofac Surg. Author manuscript; available in PMC 2017 November 12.

Published in final edited form as:

J Craniomaxillofac Surg. 2016 November ; 44(11): 1777–1785. doi:10.1016/j.jcms.2016.08.020.

Combined soft and skeletal tissue modelling of normal and dysmorphic midface postnatal development

Amel Ibrahim[a,b], **Michael Suttie**[a,c], **Neil W. Bulstrode**[a,b], **Jonathan A. Britto**[b], **David Dunaway**[a,b], **Peter Hammond**[a,c,**], and **Patrizia Ferretti**[a,*]

[a]UCL Great Ormond Street Institute of Child Health (Head: Prof. R. Smyth), University College London, London WC1N 1EH, United Kingdom

[b]Department of Plastic Surgery, Great Ormond Street Hospital NHS Trust, London WC1N 3JH, United Kingdom

[c]Nuffield Department of Obstetrics & Gynaecology, University of Oxford, Oxford OX3 7DQ, United Kingdom

Abstract

Background—Midface hypoplasia as exemplified by Treacher Collins Syndrome (TCS) can impair appearance and function. Reconstruction involves multiple invasive surgeries with variable long-term outcomes. This study aims to describe normal and dysmorphic midface postnatal development through combined modelling of skeletal and soft tissues and to develop a surgical evaluation tool.

Materials and methods—Midface skeletal and soft tissue surfaces were extracted from computed tomography scans of 52 control and 14 TCS children, then analysed using dense surface modelling. The model was used to describe midface growth, morphology, and asymmetry, then evaluate postoperative outcomes.

Results—Parameters responsible for the greatest variation in midface size and shape showed differences between TCS and controls with close alignment between skeletal and soft tissue models. TCS children exhibited midface dysmorphology and hypoplasia when compared with controls. Asymmetry was also significantly higher in TCS midfaces. Combined modelling was used to evaluate the impact of surgery in one TCS individual who showed normalisation immediately after surgery but reversion towards TCS dysmorphology after 1 year.

Conclusion—This is the first quantitative analysis of postnatal midface development using combined modelling of skeletal and soft tissues. We also provide an approach for evaluation of surgical outcomes, laying the foundations for future development of a preoperative planning tool.

Keywords

Treacher Collins syndrome; Development; Dysmorphology; Midface; Dense surface modeling; Principal component analysis

[*]Corresponding author. Stem Cells and Regenerative Medicine Section, UCL Great Ormond Street Institute of Child Health, University College London, 30 Guilford Street, London WC1N 1EH, United Kingdom. Fax: +44 020 7242 978, p.ferretti@ucl.ac.uk (P. Ferretti). [**]Corresponding author. Nuffield Department of Obstetrics & Gynaecology, University of Oxford, Oxford OX3 7DQ, United Kingdom. peter.hammond@obs-gyn.ox.ac.uk (P. Hammond).

1. Introduction

Treacher Collins Syndrome (TCS) is an autosomal dominant disorder of varying penetrance that typifies midface dysmorphia. It has a global incidence of 1:50,000 live births (Conte et al., 2011) and is caused by mutations in the TCOF1 gene. Affected children display various skeletal and soft tissue deformities; however, downward slanting palpebral fissures and zygomatic hypoplasia, which result in midface deformity, are the most consistent clinical abnormalities (Teber et al., 2004). These individuals have problems with feeding, speech, vision, and self-esteem. Reconstruction usually requires invasive procedures such as distraction-osteogenesis, foreign-body implants, and/or tissue transfer (Cobb et al., 2014). These corrections do not completely integrate or grow in harmony with the rest of the face. Thus, surgery is rarely fully or permanently restorative (Dufresne and Richtsmeier, 1995).

Three-dimensional (3D) reconstructed images from preoperative scans are currently used to plan surgery. Although this increases accuracy, it does not take into account growth and development. Craniofacial bone growth has traditionally been assessed using cephalometric studies (Bergman et al., 2014; Mellion et al., 2013) or computed tomography (CT) scans of dry skulls (Harnet et al., 2013; Nikkhah et al., 2013), or indirectly by extrapolating data from soft tissue to the underlying skeleton (Krimmel et al., 2015). Reliance on plain radiographs or CT scans has limited the number of studies that could be undertaken in healthy children who do not normally have such imaging. In contrast, soft tissue growth and morphology has been extensively studied in normal and abnormal development, as measurements can be easily obtained through anthropometrics (Farkas et al., 1992; Tutkuviene et al., 2015) or surface modelling using 3D imaging (De Souza et al., 2013; Koudelová et al., 2015; Suttie et al., 2013). Craniofacial shape and variation can be quantified using morphometric analysis (MA), which has been widely used to study heterogeneity in soft tissues of the face, classify non-genetic diseases, demonstrate normal growth and facial asymmetry, and link gene expression to facial phenotype (De Souza et al., 2013; Hammond et al., 2003; Hopman et al., 2014). Although quantitative analysis of the facial skeletal tissues for preoperative planning has been undertaken in TCS, this only used cephalometric analysis or focused on mild dysmorphism (Chong et al., 2008; Nikkhah et al., 2013). Hence, computer-aided modelling of severe TCS defects and of the relationship between skeletal and soft tissue shape and growth is still needed to evaluate the efficacy of surgery and plan reconstruction.

This study aims to provide a quantitative description of growth and symmetry of normal midface development and to assess how this is affected in TCS using the relatively large number of craniofacial CT scans available at Great Ormond Street Hospital (GOSH). We used MA to model the relationship between the shape of skeletal and soft tissues during postnatal midface development. This will form the basis for developing more accurate tools for evaluating and planning midface reconstructive surgery.

2. Methods

2.1. Patient inclusion

Retrospectively collected, anonymised CT scans of the face of control and TCS children were acquired from the radiology department at GOSH. Controls were patients coded as not having craniofacial defects and had undergone CT scanning of the head for other reasons (e.g., vascular malformation, oncology, or otorhinolaryngology). Children with TCS were identified through international diagnostic clinical codes for the disease and clinic letters cross-checked to ensure that diagnosis was accurate. Confirmation was obtained through the National Research Ethics Service that the study did not require Research Ethics Committee approval, as it fulfilled their criteria for "projects using non identifiable data that was routinely collected not for research."

2.2. Image processing and extraction of surfaces

CT scans were converted to DICOM format using OSIRIX©. Those unsuitable for analysis (e.g., incomplete imaging of the face) were excluded. 3D STL files of the bone and soft tissue were extracted simultaneously using Invesalius© using constant thresholds for volume rendering of bone or soft tissue. These were then edited using Meshlab© and VAM© to obtain individual surfaces.

2.3. Generation of landmarks

Anatomically constant landmarks of the skeletal and soft tissue were identified through review of anatomical textbooks (Gray et al., 2005) and the literature (Hopman et al., 2014; Nikkhah et al., 2013) to ensure chosen landmark reliability and reproducibility. The majority of soft tissue landmarks used were similar to those described previously (Suttie et al., 2013). A new pair of soft tissue landmarks, right and left temporale, were generated by superimposing soft and skeletal tissue surfaces, then selecting the soft tissue point directly overlying the temporal fossa. Discrete skeletal landmarks for the zygoma and adjacent maxilla as well as lower portion of the frontal bones were identified using direct and indirect landmarking (Farkas et al., 2004, 1999, 2002).

2.4. Cephalometric measurements of skeletal and soft tissue CT scan reconstructions

Indirect (cephalometric) measurements of midface width, depth, and length were performed by extracting (using software developed in-house) the Euclidean distance between landmarks identified as representative of midface width, length, and depth (Budai et al., 2003; Farkas et al., 1992, 2002; Kolar et al., 1985).

2.5. Building of dense surface models

Skeletal and soft tissue landmarks (Table 1; Supplementary Fig. S1) were used to annotate each of the respective surfaces using software developed in-house Facemark© (Suttie et al., 2013) by one individual (A.I.) and cross-checked by another (M.S.).

Using the Procrustes algorithm to compute mean landmarks and thin-plate splines, face/skull surfaces were warped to the mean landmarks, which enabled the set of face/skull surfaces to be closely aligned. This allowed points on a selected face/skull to be mapped to the closest

points on all others to induce a dense surface correspondence of tens of thousands of points, enabling computation of the mean midface surface (skeletal or soft). Position differences between the densely corresponded points on each midface surface and those on the mean midface were subjected to principal component analysis (PCA). Principal components (PCs) accounting for 99% of face variation were used to build a 3D dense surface model (DSM) for synthesis of midface structures (Hopman et al., 2014) for skeletal and soft tissues.

2.6. Reflection–original analysis

Facial asymmetry analysis involved generating a reflected form of each surface and relabelling left–right landmarks before building a DSM of original and reflected midface surfaces (Hammond et al., 2008). The Euclidean distance between the DSM representations of the original and reflected faces was used to estimate asymmetry.

2.7. Statistical analysis

GraphPad Prism software was used to generate all charts and graphs apart from 3D scatter plots, which were created using SPSS. Linear regression analysis was used to compare the differences between TCS and control children with respect to the first two PCs in the skeletal and soft tissue DSM as well as the asymmetry index. P values were calculated to test whether differences between slopes and intercepts of the regression lines of the TCS and Control subgroups were significantly different ($p < 0.05$). Bootstrapping was used to generate confidence intervals for the asymmetry index values in SPSS. An unpaired 2-tailed t-test with Welch's correction was used to analyse the mean difference of asymmetry indices and cephalometric measures between the TCS and control subgroups ($p < 0.05$).

3. Results

3.1. Sample characteristics and landmarks used for DSM building

A total of 68 CT scans of patients (52 controls, 14 preoperative TCS, and 2 postoperative TCS) were used to extract a soft tissue and skeletal tissue surface for each patient in this study (Fig. 1; Table 1; Supplementary Fig. S1). The gender ratio was 28:23 (male:female) in the control group and 8:6 in the TCS preoperative group. Age was distributed from 1 to 16 years (Figure, Supplementary Fig. S2). One TCS boy had a preoperative (aged 13), immediately postoperative (aged 14), and 1-year postoperative CT scan (aged 15).

A total of 45 skeletal and 24 soft tissue landmarks were used to annotate each skeletal and soft tissue surface, respectively, building separate skeletal, soft tissue, and combined DSMs (Fig. 1; Table 1; Supplementary Fig. S2).

3.2. Combined modelling reveals close alignment between skeletal and soft tissue morphology

The first PC (PC1) was responsible for 54%, 58%, and 54% of variation in the skeletal, soft tissue, and combined models, respectively. When plotted against age, PC1 corresponds to overall midface growth (length and width) (Fig. 2A; Video 1). In the skeletal model, the PC1-age regression line has a significantly non-zero slope in controls (slope = 0.1795 ± 0.0104, $p < 0.0001$) and TCS (slope = 0.1727 ± 0.03917, $p = 0.0009$) indicating a linear

relationship between age and PC1. The difference in slopes is not significant ($p = 0.8152$) suggesting similar rates of growth for both groups, whereas the difference in the intercepts ($p < 0.0001$) reflects reduced midface size in TCS. In the soft tissue model, there is also a linear relationship between age and PC1 (slope = 0.1928 ± 0.0102; $p < 0.0001$) in controls and TCS (slope = 0.1383 ± 0.05277; $p = 0.0224$), again with similar slopes ($p = 0.1056$) but differing intercepts ($p = 0.0003$). In the combined model, PC1 also relates to age in controls (slope = 0.1896 ± 0.009142, $p < 0.0001$) and TCS (slope = 0.1639 ± 0.04472, $p = 0.0032$) with lack of difference in slopes ($p = 0.3756$) and significant difference in intercepts ($p < 0.0001$).

Supplementary data related to this article can be found online at http://dx.doi.org/10.1016/j.jcms.2016.08.020.

PC2 mainly relates to midface width and depth (Fig. 2B; Video 2) and accounts for 11%, 12%, and 11% of variation in the skeletal, soft tissue, and combined models, respectively. In the skeletal model, the linear regression line for controls has a significantly non-zero slope (slope = -0.05733 ± 0.01102, $p < 0.0001$) indicating a direct relationship between age and PC2 which is not the case for TCS (slope = -0.03037 ± 0.07958, $p = 0.7094$). Controls and TCS do not show significant difference in regression line slope ($p = 0.5516$) but do so for intercept ($p < 0.0001$) likely due to the narrower and shallower midface in TCS. The soft tissue DSM reveals a significant relationship between age and PC2 for controls (slope = -0.07150 ± 0.01841, $p = 0.0003$) but not for TCS (slope = -0.04613 ± 0.06012, $p = 0.4577$) with similar slopes ($p = 0.5986$) but different intercepts ($p < 0.0001$). The combined DSM is consistent with the skeletal and soft tissue models demonstrating a linear relationship between age and PC2 in controls (slope = -0.06683 ± 0.01370, $p < 0.0001$) but not TCS (slope = -0.05497 ± 0.07358, $p = 0.4694$) without significant differences between TCS and control slopes ($p = 0.7961$) and significant difference in intercepts ($p < 0.0001$).

Supplementary data related to this article can be found online at http://dx.doi.org/10.1016/j.jcms.2016.08.020.

Bivariate analysis of the first two PCs supports the relationship between skeletal and soft tissue growth and morphology ($p < 0.0001$) shown by the DSM (Supplementary Fig. S3).

PC3 describes mainly midface width and length (Video 3). Along with PC1 and PC2, the first three PCs account for 70%, 79%, and 71% of all shape variation in the skeletal, soft tissue, and combined models (Videos 1–3). A 3–d scatter plot (Fig. 2C) of PC1-3 shows separate clustering of controls and TCS but overlap of 5 TCS individuals who are located within or close to the control data set, likely reflecting phenotypic heterogeneity. The similar appearance of the scatter plots of all three DSM suggests that skeletal and soft tissue midface morphology is closely aligned with respect to PC1-3.

Supplementary data related to this article can be found online at http://dx.doi.org/10.1016/j.jcms.2016.08.020.

3.3. Heat maps reveal shape differences in the TCS midface

Heat maps were used to compare a 4-year-old child with TCS to age-sex-ethnicity–matched controls (n = 20) and to visually represent the differences described by the DSM (Fig. 3A). In the surface normal comparison, the zygomatic and temporal bone regions in the skeletal model and corresponding soft tissue areas (malar and bitemporal) demonstrate malar hypoplasia and bitemporal narrowing (red in Fig. 3A), whereas frontal and nasal regions in both models illustrate prominence of the nose (blue in Fig. 3A) and relatively (compared with malar region) enlarged forehead, which are characteristic of TCS (Kolar et al., 1985). In the lateral (X-axis) and vertical (Y-axis) comparisons, there is midface narrowing and shortening, respectively (red in Fig. 3A). Along the depth (Z-axis), the fronto-nasal region shows reduction in depth (red in Fig. 3A). As a whole, this individual exhibits midfacial, orbital, and zygomatic hypoplasia that is typical of TCS dysmorphism (Kolar et al., 1985, 1987). These typical features were similarly demonstrated using a dynamic morph of an older 12 year-old TCS individual (Video 4).

Supplementary data related to this article can be found online at http://dx.doi.org/10.1016/j.jcms.2016.08.020.

The average TCS midface was generated using the means of the PC values for all of the TCS models and compared with age-sex-ethnicity–matched controls (n = 14) to generate a heat map (Fig. 3B). The corresponding soft tissue areas reflect malar hypoplasia in the surface comparison (red-yellow in Fig. 3B). Enlargement of the fronto-nasal area in the skeletal model corresponds with the relative enlargement of the forehead and prominent nose (blue in Fig. 3B) in the soft tissue heat map. Along the X-axis, there is zygomatic narrowing in the skeletal model, whereas both skeletal and soft tissue models reveal shortening (red in Fig. 3B) along the Y-axis.

3.4. Cephalometric analysis of midface soft and skeletal tissue surfaces supports DSM findings

To validate our models, we analysed cephalometric measurements of midface size (width, length, and depth) (Table 2, Fig. 1). Analysis demonstrates reduction in width of unoperated TCS midfaces compared with controls in both skeletal ($p = 0.0033$) and soft tissue models ($p = 0.0009$). Midface depth is also significantly different in skeletal (<0.0001) and soft tissue (<0.0001) measurements.

3.5. Comparison of preoperative, immediately postoperative, and one-year-postoperative TCS

Heat maps of a male individual with Treacher Collins syndrome reveal zygomatic hypoplasia preoperatively with corresponding loss of soft tissue volume in the malar region (red in Fig. 3C(a)) compared with age-sex-ethnicity–matched controls (n = 20). This patient underwent reconstruction with bone grafts, and immediate results showed improvement in the skeletal and soft tissue hypoplasia (blue-green in Fig. 3C(b)). One year later, the zygomatic bones are corrected but beginning to resorb (green-yellow-red in Fig. 3C(c)) and soft tissue appears hypoplastic (red in Fig. 3C(c)) compared with immediately postoperative.

This reversion of midface morphology is also reflected in the 3D scatterplots of PC1-3 (Fig. 2C). The preoperative TCS individual is initially located among the TCS cluster of patients in all three scatterplots. Immediately postoperatively, this individual moves closer to the normal dataset within the plot, but 1 year post-operatively, he regresses towards the TCS cluster.

3.6. Asymmetry of the midface is increased in TCS

The difference of the PCA representations of original and reflected forms was used to visualize and measure asymmetry of the midface in each individual (Fig. 2D). The mean asymmetry index of the midface in the TCS subgroup is significantly higher than in controls in the skeletal ($p < 0.0001$) and soft tissue ($p < 0.0001$) models. The mean asymmetry index of controls (skeletal = 123, Soft tissue = 87.59) was compared with that of TCS (skeletal = 197.8, soft tissue = 123) and demonstrated differences in both skeletal ($p = 0.0018$) and soft tissues ($p = 0.0033$) (Table 3). Bootstrap confidence intervals for these comparisons did not show any possible correlation.

4. Discussion

This study is the first to describe facial growth and morphology in a healthy and syndromic paediatric population using combined skeletal and soft tissue modelling. This builds on the work of Liebregts et al., who showed that surfaces acquired from pre- and postoperative CT images can be used to plan mandibular advancement surgery (Liebregts et al., 2015a, b). Their study accurately predicted soft tissue changes postsurgery and was validated in another paper published by this group using the same technique to plan bimaxillary correction (Liebregts et al., 2015a, b). These papers provide important evidence supporting virtual planning of surgery but are limited to nonsyndromic adults and adolescents. More recently, Young et al. also used CT images to extract soft tissue and skeletal 3D surfaces of the face in patients aged 7 to 58 (n = 175) (Young et al., 2016). Using geometric morphometrics, they analysed skeletal and soft tissue shape to show significant covariation, providing evidence that skeletal shape can be predicted using soft tissue morphology. Although we also built our models using CT reconstructions of skeletal and soft tissue surfaces, we show close alignment between morphology of the midface skeleton and its soft tissue envelope using individual and combined DSM for normal and TCS midface postnatal development. Through this we have quantified changes in midface width, depth, and size to describe the skeletal and soft tissue defects in TCS. We also found evidence of significant midfacial asymmetry in TCS not previously reported (Dixon, 1996). Our results are supported by the findings of anthropometric studies of the face by Kolar et al. (1985), who demonstrated reduced face width, reduced depth, and normal length in TCS. Although they concisely described the dysmorphism in TCS using well-established protocols, their study included only 6 children and was restricted to soft tissue morphology. Skeletal dysmorphism in TCS was previously analysed by Nikkhah et al. (2013), who used cephalometric measurements on preoperative CT scans of TCS and control (dry) skulls, which were then compared using PCA to quantify the dysmorphism in TCS and to attempt virtual normalization. Their study analysed only skeletal models and excluded severe defects. An attempt at correlating skeletal and soft tissue findings in TCS was made by Herlin et al.

(2013a, b), who used CT reconstructions for skeletal analysis and magnetic resonance imaging (MRI) for the soft tissue study (Herlin et al., 2013a, b) to perform surgical simulation. Although this presented the first quantitative analysis of subcutaneous soft tissue volume in TCS, limitations included a small sample size on the MRI study (n = 2 TCS) and methodology that disallowed direct correlation between skeletal and soft tissues. Additionally, we used our model to compare a pre- and postoperative TCS patient against controls to evaluate the efficacy of surgery. This demonstrated immediate correction that was not maintained at 1 year. More CT scans are required to assess whether this is due to the type of surgery performed or to limitations in preoperative planning tools, and whether there will be ongoing reversion to TCS phenotype.

Our study is limited by the relatively small sample size, especially with regards to the postoperative evaluation patient (n = 1). An increased sample size, different surgical procedures, and most importantly repeat CT scan data for each individual over a prolonged period of time are needed to build a tool that can model growth trajectories for each child. This would allow identification of the most variable regions in face growth and shape and correlation between the dependent variables. The combined model needs further analysis to accurately assess how it correlates with the individual DSM, to understand how changes to the skeletal DSM affect the soft tissue and the reverse. This would permit the development of a surgical planning tool with adequate predictive capabilities so that immediate and long-term morphology and growth can be simulated. The increase in sample size and longitudinal data collection is more easily achievable in the TCS cohort who often have repeat scans but may be difficult with regards to controls; thus a multi-centre study will be necessary.

5. Conclusion

This study shows that a combined model can be generated to relate skeletal and soft tissue changes during normal and TCS midface postnatal development. Heat maps and PCA were used to describe the dysmorphism in TCS and to evaluate the impact of a common surgical procedure, revealing that although correction may be achieved in the short term, it may not be maintained in the long term. This combined approach could eventually be used to develop a surgical planning tool, and extended to other parts of the face using similar protocols.

Supplementary Material

Refer to Web version on PubMed Central for supplementary material.

Acknowledgments

We would also like to thank Mr Simon Hadley (Great Ormond Street Hospital) and Dr Tharsika Karunakaran for their help in obtaining the initial CT scans for this study.

Funding source

This work was funded by the RCS Blond Surgical Research Fellowship (AI) and the National Institute on Alcohol Abuse and Alcoholism (PH and MS: 2U01AA014809). It was also supported by the National Institute for Health Research Biomedical Research Centre at Great Ormond Street Hospital for Children, NHS Foundation Trust and University College London.

Appendix A. Supplementary data

Supplementary data related to this article can be found at http://dx.doi.org/10.1016/j.jcms.2016.08.020.

References

Bergman RT, Waschak J, Borzabadi-Farahani A, Murphy NC. Longitudinal study of cephalometric soft tissue profile traits between the ages of 6 and 18 years. Angle Orthod. 2014; 84(1):48–55. [PubMed: 23834271]

Budai M, Farkas LG, Tompson B, Katic M, Forrest CR. Relation between anthropometric and cephalometric measurements and proportions of the face of healthy young white adult men and women. J Craniofac Surg. 2003; 14(2):154–161. discussion 162–153. [PubMed: 12621284]

Chong DK, Murray DJ, Britto JA, Tompson B, Forrest CR, Phillips JH. A cephalometric analysis of maxillary and mandibular parameters in Treacher Collins syndrome. Plast Reconstr Surg. 2008; 121(3):77e–84e.

Cobb AR, Green B, Gill D, Ayliffe P, Lloyd TW, Bulstrode N, et al. The surgical management of Treacher Collins syndrome. Br J Oral Maxillofac Surg. 2014; 52(7):581–589. [PubMed: 24776174]

Conte C, D'Apice MR, Rinaldi F, Gambardella S, Sangiuolo F, Novelli G. Novel mutations of TCOF1 gene in European patients with Treacher Collins syndrome. BMC Med Genet. 2011; 12:125. [PubMed: 21951868]

de Souza MA, McAllister C, Suttie M, Perrotta C, Mattina T, Faravelli F, et al. Growth hormone, gender and face shape in Prader-Willi syndrome. Am J Med Genet A. 2013; 161(10):2453–2463.

Dixon MJ. Treacher Collins syndrome. Hum Mol Genet. 1996; 5:1391–1396. Spec. [PubMed: 8875242]

Dufresne C, Richtsmeier JT. Interaction of craniofacial dysmorphology, growth, and prediction of surgical outcome. J Craniofac Surg. 1995; 6(4):270–281. [PubMed: 9020701]

Farkas LG, Eiben OG, Sivkov S, Tompson B, Katic MJ, Forrest CR. Anthropometric measurements of the facial framework in adulthood: age-related changes in eight age categories in 600 healthy white North Americans of European ancestry from 16 to 90 years of age. J Craniofac Surg. 2004; 15(2): 288–298. [PubMed: 15167252]

Farkas LG, Posnick JC, Hreczko TM. Growth patterns of the face: a morphometric study. Cleft Palate Craniofac J. 1992; 29(4):308–315. [PubMed: 1643058]

Farkas LG, Tompson B, Phillips JH, Katic MJ, Cornfoot ML. Comparison of anthropometric and cephalometric measurements of the adult face. J Craniofac Surg. 1999; 10(1):18–25. discussion 26. [PubMed: 10388422]

Farkas LG, Tompson BD, Katic MJ, Forrest CR. Differences between direct (anthropometric) and indirect (cephalometric) measurements of the skull. J Craniofac Surg. 2002; 13(1):105–108. discussion 109–110. [PubMed: 11887005]

Gray H, Standring S, Ellis H, Berkovitz BKB. Gray's anatomy: the anatomical basis of clinical practice. Elsevier Churchill Livingstone. 2005

Hammond P, Forster-Gibson C, Chudley AE, Allanson JE, Hutton TJ, Farrell SA, et al. Face-brain asymmetry in autism spectrum disorders. Mol Psychiatry. 2008; 13(6):614–623. [PubMed: 18317467]

Hammond P, Hutton T, Maheswaran S, Modgil S. Computational models of oral and craniofacial development, growth, and repair. Adv Dent Res. 2003; 17:61–64. [PubMed: 15126209]

Harnet JC, Lombardi T, Maniere-Ezvan A, Chamorey E, Kahn JL. Transversal craniofacial growth evaluated on children dry skulls using V2 and V 3 canal openings as references. Surg Radiol Anat. 2013; 35(9):757–763. [PubMed: 23625072]

Herlin C, Doucet JC, Bigorre M, Captier G. Computer-assisted midface reconstruction in Treacher Collins syndrome part 2: soft tissue reconstruction. J Craniomaxillofac Surg. 2013a; 41(7):676–680. [PubMed: 23465636]

Herlin C, Doucet JC, Bigorre M, Khelifa HC, Captier G. Computer-assisted midface reconstruction in Treacher Collins syndrome part 1: skeletal reconstruction. J Craniomaxillofac Surg. 2013b; 41(7): 670–675. [PubMed: 23454266]

Hopman SM, Merks JH, Suttie M, Hennekam RC, Hammond P. Face shape differs in phylogenetically related populations. Eur J Hum Genet. 2014; 22(11):1268–1271. [PubMed: 24398794]

Kolar JC, Farkas LG, Munro IR. Surface morphology in Treacher Collins syndrome: an anthropometric study. Cleft Palate J. 1985; 22(4):266–274. [PubMed: 3863724]

Kolar JC, Munro IR, Farkas LG. Anthropometric evaluation of dysmorphology in craniofacial anomalies: Treacher Collins syndrome. Am J Phys Anthropol. 1987; 74(4):441–451. [PubMed: 3442295]

Koudelova J, Dupej J, Br u zek J, Sedlak P, Velemínsk a J. Modelling of facial growth in Czech children based on longitudinal data: age progression from 12 to 15 years using 3D surface models. Forensic Sci Int. 2015; 248:33–40. [PubMed: 25576677]

Krimmel M, Breidt M, Bacher M, Müller-Hagedorn S, Dietz K, Bülthoff H, et al. Three-dimensional normal facial growth from birth to the age of 7 years. Plast Reconstr Surg. 2015; 136(4):490e–501e.

Liebregts J, Xi T, Timmermans M, de Koning M, Berge S, Hoppenreijs T, et al. Accuracy of three-dimensional soft tissue simulation in bimaxillary osteotomies. J Craniomaxillofac Surg. 2015a; 43(3):329–335. [PubMed: 25637495]

Liebregts JH, Timmermans M, De Koning MJ, Berge SJ, Maal TJ. Three-dimensional facial simulation in bilateral sagittal split osteotomy: a validation study of 100 patients. J Oral Maxillofac Surg. 2015b; 73(5):961–970. [PubMed: 25795178]

Mellion ZJ, Behrents RG, Johnston LE. The pattern of facial skeletal growth and its relationship to various common indexes of maturation. Am J Orthod Dentofacial Orthop. 2013; 143(6):845–854. [PubMed: 23726335]

Nikkhah D, Ponniah A, Ruff C, Dunaway D. Planning surgical reconstruction in Treacher-Collins syndrome using virtual simulation. Plast Reconstr Surg. 2013; 132(5):790e–805e.

Suttie M, Foroud T, Wetherill L, Jacobson JL, Molteno CD, Meintjes EM, et al. Facial dysmorphism across the fetal alcohol spectrum. Pediatrics. 2013; 131(3):e779–788. [PubMed: 23439907]

Teber OA, Gillessen-Kaesbach G, Fischer S, Böhringer S, Albrecht B, Albert A, et al. Genotyping in 46 patients with tentative diagnosis of Treacher Collins syndrome revealed unexpected phenotypic variation. Eur J Hum Genet. 2004; 12(11):879–890. [PubMed: 15340364]

Tutkuviene, J., Cattaneo, C., Obertov a, Z., Ratnayake, M., Poppa, P., Barkus, A., et al. Age-and sex-related growth patterns of the craniofacial complex in European children aged 3–6 years; Ann Hum Biol. 2015. p. 1-10.http://dx.doi.org/10.3109/03014460.2015.1106584

Young NM, Sherathiya K, Gutierrez L, Nguyen E, Bekmezian S, Huang JC, et al. Facial surface morphology predicts variation in internal skeletal shape. Am J Orthod Dentofacial Orthop. 2016; 149(4):501–508. [PubMed: 27021454]

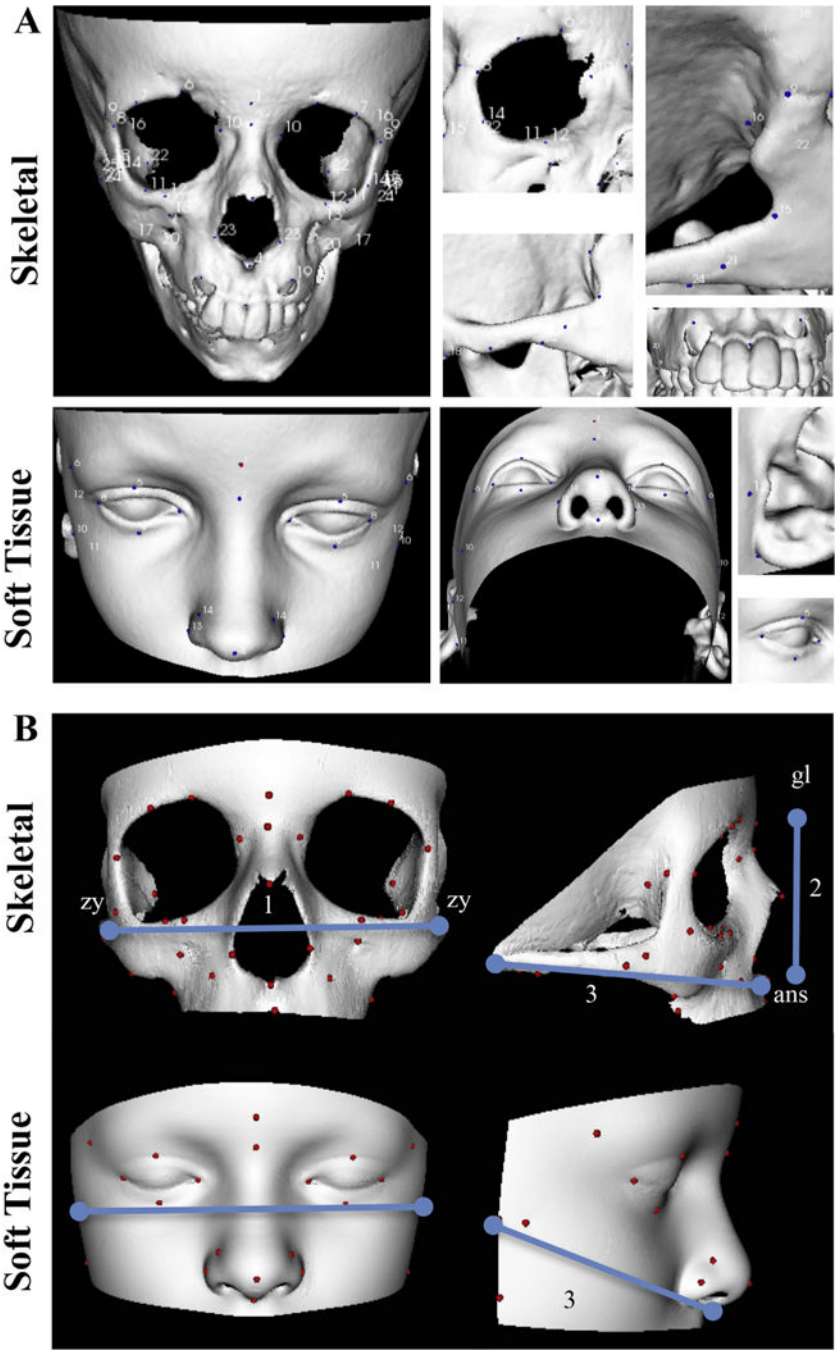

Fig. 1.

Skeletal and soft tissue 3D reconstructed CT scans annotation. A) Skeletal and soft tissue 3D reconstructions annotated with landmarks described in Table 1. B) Landmarking for cephalometric measurements. 1: width (zy-zy). 2: length (skeletal: gl-ans; soft tissue: gl-sn). 3: depth (skeletal: ans-m; soft tissue: sn-p); *ans: anterior nasal spine, gl: glabella, m: mastoidale, na: nasion, p: preaurale, sn: subnasale, zy: zygion*.

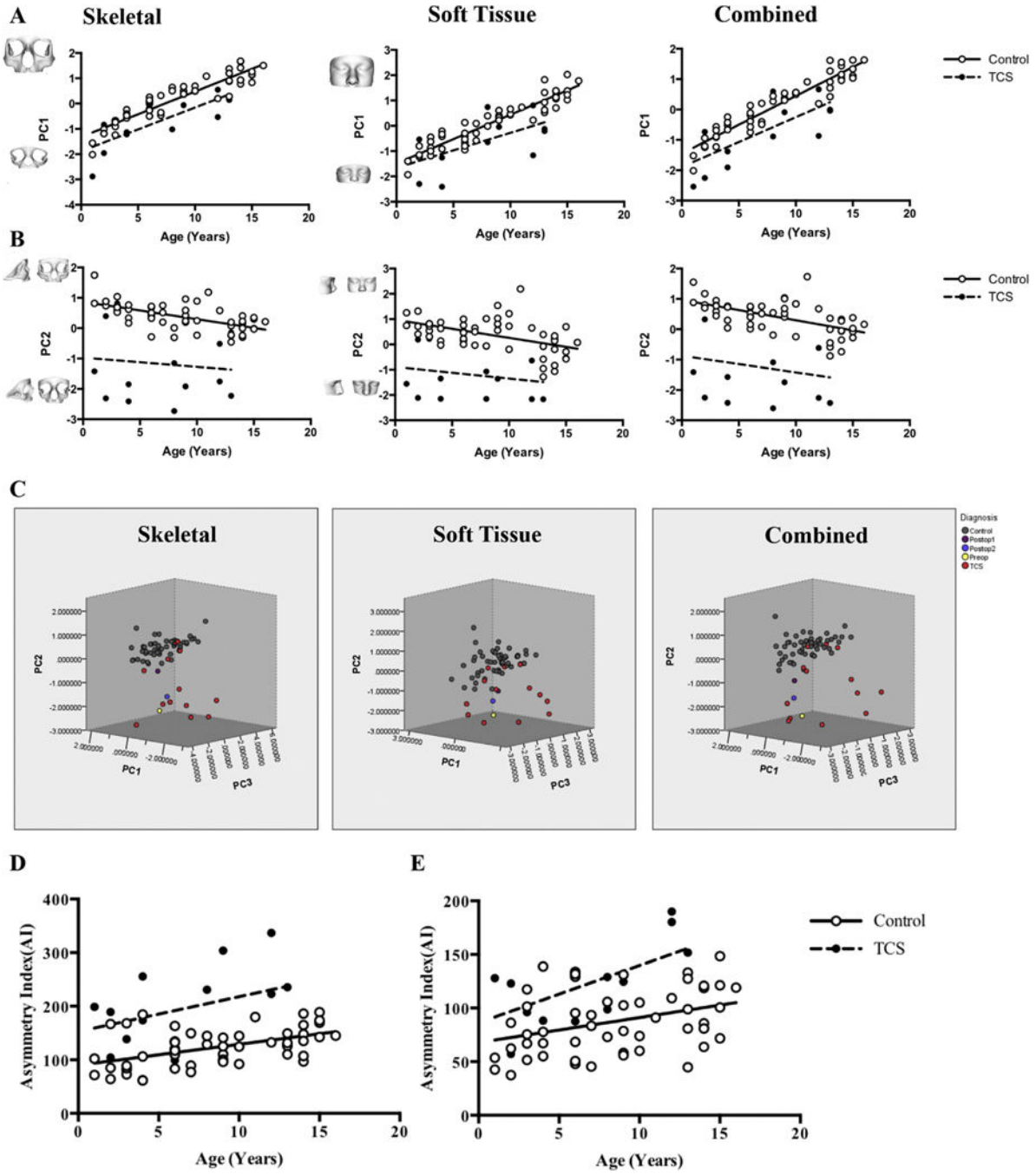

Fig. 2.

Comparison of midface morphometry and asymmetry. A) Growth as indicated by PC1 is reduced in TCS on skeletal ($p < 0.0001$), soft tissue ($p = 0.0003$) and combined ($p < 0.0001$) DSM. B) Width and depth indicated by PC2 is reduced in TCS on skeletal ($p < 0.0001$), soft tissue ($p < 0.0001$), and combined ($p < 0.0001$) DSM. C) Comparison of pre-and postoperative TCS midfaces using the first three PCs shows separate clustering of TCS and control groups. The preoperative TCS (preop) patient (located among TCS group) moves closer to the controls postoperatively (Postop 1) but regresses to the TCS cluster 1 year

postoperatively (Postop 2). D and E) Comparison of midface asymmetry between TCS and controls using linear regression analysis of the asymmetry index (AI). Note increased AI in TCS in (D) skeletal tissues ($p < 0.0001$) and (E) corresponding increase in soft tissue asymmetry of TCS midfaces ($p < 0.0001$).

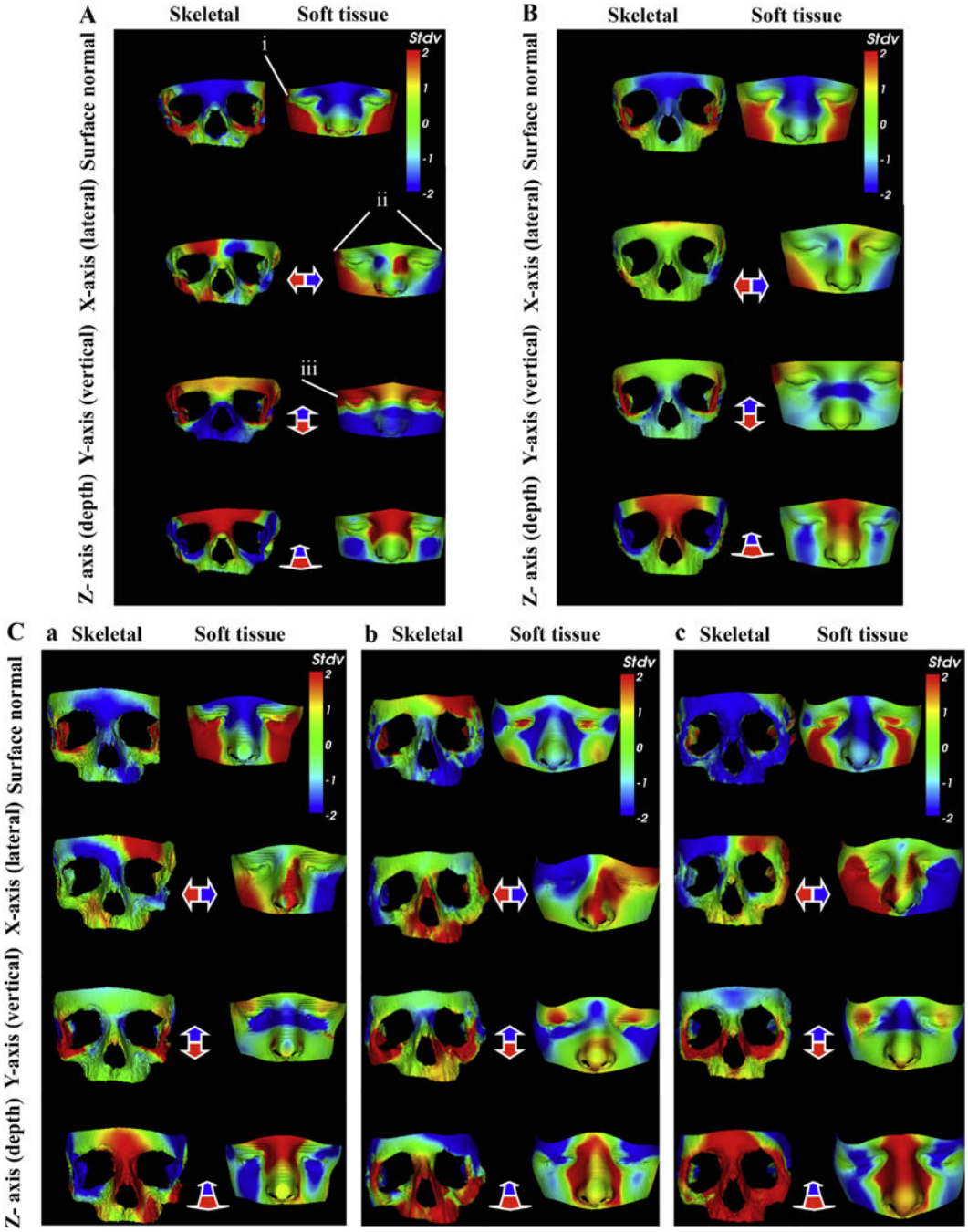

Fig. 3.

Heat map visualisation of TCS midface dysmorphism compared with controls. A) Dysmorphology in a 4-year old with TCS produces zygomatic and malar hypoplasia (red-yellow), bitemporal narrowing (red on surface normal (i); red-blue on lateral (ii)) and down-slanting palpebral fissures (red on vertical (iii)). B) The average TCS midface (n = 14) exhibits narrowing and shortening of the zygoma (X and Y-axes) and reduction in fronto-nasal depth (Z-axis). Surface normal shows malar and zygomatic hypoplasia (yellow-red), increased interorbital distance (blue) and nasal bridge prominence (blue). C) Evaluating

surgery in a TCS child: a) Preoperatively there is zygomatic (skeletal), malar, orbital, and bitemporal (soft tissue) hypoplasia. b) Dysmorphology reduces after surgery. c) One year postoperatively there is soft tissue malar and bitemporal hypoplasia compared with (b), but improved overall compared with preop (a). Controls (n = 20). Heat maps demonstrate difference between TCS and controls on surface normal comparison and along the X, Y, and Z axes. Red-green-blue scale indicates a contraction-coincidence-expansion of 2 standard deviations (Stdv) from the mean in the surface-normal comparison.

Table 1

Description of landmarks used to annotate midface surfaces.

	Skeletal landmark	Definition
Unpaired	1. Glabella	Midway between the supraorbital notches
	2. Nasion	Midpoint of frontonasal suture
	3. Rhinion	Most anterior-inferior point of nasal suture
	4. Anterior nasal spine	Apex of anterior nasal spine of maxilla
	5. Interdentale superius	Between the upper two incisors
Paired	6. Supraorbital foramen	Most concave point of supraorbital notch
	7. Supraorbital margin	Midpoint of the orbital rim
	8. Anterior frontozygomatic	Most anterior point of frontozygomatic suture
	9. Posterior frontozygomatic	Most posterior point of frontozygomatic suture
	10. Lateral frontonasal suture	Most lateral point of frontonasal suture
	11. Orbitale	Most inferior portion of lower orbital rim
	12. Maxillary process	Most superior part of zygomaticomaxillary suture
	13. Infraorbital foramen	Most concave point below infraorbital margin
	14. Ectoconchion	Point of maximum breadth on lateral wall of orbit
	15. Jugale	Junction of the temporal and frontal processes
	16. Infratemporal fossa	Midpoint of cavity deep to Zygommatic arch
	17. Zygomaxillare	Most inferior tip of zygomaticomaxillary suture
	18. Mastoidale	Lowest point on the contour of the mastoid process
	19. Canine fossa	Depression lateral to canine eminence
	20. Tuberosity of maxilla	Lowest part of the infratemporal surface of maxilla
	21. Zygion	Most lateral point on outline of Zygoma
	22. Inferior orbital fissure	Apex of sphenomaxillary suture
	23. Alare	Most lateral point of nasal aperture
	24. Articular tubercle	Inferior and proximal eminence of zygomatic process
	25. Postglenoid tubercle	Inferior distal projection of zygomatic process
	Soft tissue landmark	Definition
Unpaired	1. Glabella	Most prominent point of frontal bone in the midline
	2. Nasion[a]	Midline of frontonasal suture
	3. Pronasale	Most prominent point on nasal tip
	4. Subnasale	Midpoint of columella base
Paired	5. Palpebrae superius	Midpoint of superior aspect of palpebral fissure
	6. Frontotemporale[a]	Concavity above supraorbital rim
	7. Endocanthion	Most medial point of palpebral fissure
	8. Exocanthion	Most lateral point of palpebral fissure
	9. Palpebrae Inferius	Midpoint of inferior aspect of palpebral fissure
	10. Zygion[a]	Most lateral extents of zygoma
	11. Subaurale	Most inferior point of the free auricular margin
	12. Preaurale	Most anterior part of the ear

Skeletal landmark	Definition
13. Alare	Lateral extent of alar contour
14. Lateral pronasale	Most distal point of alar groove

[a]Landmarks were obtained by superimposing soft tissue surface onto skeletal and projecting the landmark (see Supplementary Fig. S1).

Table 2

Differences in cephalometric measurements between control and Treacher Collins (TCS) midface reconstructions.

Measurements (corresponding landmarks)	Skeletal			Soft tissue		
	Controls (n = 52)	Unoperated TCS (n = 14)	p-values	Controls (n = 52)	Unoperated TCS (n = 14)	p-values
Midface width (zy-zy)	106.8 ± 1.279	90.55 ± 4.475	0.0033[b]	125.0 ± 2.828	102.1 ± 5.194	0.0009[b]
Midface length (Soft tissue: gl-sn; Skeletal: gl-ans)	51.80 ± 0.9531	48.46 ± 2.116	0.1665	58.08 ± 1.199	54.75 ± 2.682	0.2714
Midface depth[a] (Soft tissue: sn-p; Skeletal: ans-m)	91.24 ± 1.018	81.09 ± 1.939	<0.0001[b]	108.0 ± 1.150	92.13 ± 2.056	<0.0001[b]

[a]For depth both left and right-sided measurements were analysed. The landmarks are as defined in Table 1 (**ans**: anterior nasal spine, **gl**: glabella, **m**: mastoidale, **na**: nasion, **p**: preaurale, **sn**: subnasale, **zy**: zygion). Values shown are means ± (standard error of mean) SEM.

[b]Statistically significant; p-values are from unpaired two-tailed t-test.

Table 3

Comparison of the mean asymmetry indexes of the control and Treacher Collins Syndrome (TCS) groups in the skeletal and soft tissue models and bootstrap confidence intervals.

Group	Skeletal			Soft tissue		
	Controls (n = 52)	Unoperated TCS (n = 14)	p-value	Controls (n = 52)	Unoperated TCS (n = 14)	p-value
Mean ± SEM	123.00 ± 4.89	197.80 ± 19.11	0.0018[a]	87.59 ± 4.14	123.3 ± 9.697	0.0033[a]
BCa 95% LCI	113.83	164.28	NA	79.09	107.3732	NA
BCa 95% UCI	131.55	232.55	NA	95.85	140.3852	NA

BCa: Bias-corrected and accelerated; LCI: Lower Confidence Interval ± (standard deviations) STD; Upper Confidence Interval ± STD.

[a]Statistically significant (unpaired two-tailed t-test).